

# The $m = 1$ instability & gravitational wave signal in binary neutron star mergers

Luis Lehner,<sup>1</sup> Steven L. Liebling,<sup>2</sup> Carlos Palenzuela,<sup>3</sup> and Patrick M. Motl<sup>4</sup>

<sup>1</sup>*Perimeter Institute for Theoretical Physics, Waterloo, Ontario N2L 2 Y5, Canada*

<sup>2</sup>*Department of Physics, Long Island University, Brookville, New York 11548, USA*

<sup>3</sup>*Departament de Física, Universitat de les Illes Balears and Institut*

*d'Estudis Espacials e Catalunya, Palma de Mallorca, Balears E-07122, Spain*

<sup>4</sup>*School of Sciences, Indiana University Kokomo, Kokomo, IN 46904, USA*

(Dated: April 3, 2018)

We examine the development and detectability of the  $m = 1$  instability in the remnant of binary neutron star mergers. The detection of the gravitational mode associated with the  $m = 1$  degree of freedom could potentially reveal details of the equation of state. We analyze the post-merger epoch of simulations of both equal and non-equal mass neutron star mergers using three realistic, microphysical equations of state and neutrino cooling. Our studies show such an instability develops generically and within a short dynamical time to strengths that are comparable or stronger than the  $m = 2$  mode which is the strongest during the early post-merger stage. We estimate the signal to noise ratio that might be obtained for the  $m = 1$  mode and discuss the prospects for observing this signal with available Earth-based detectors. Because the  $m = 1$  occurs at roughly half the frequency of the more powerful  $m = 2$  signal and because it can potentially be long-lived, targeted searches could be devised to observe it. We estimate that with constant amplitude direct detection of the mode could occur up to a distance of roughly 14 Mpc whereas a search triggered by the inspiral signal could extend this distance to roughly 100 Mpc.

## Contents

<b>I. Introduction</b>	1
<b>II. Numerical Implementation</b>	2
<b>III. Results: Density behavior &amp; gravitational waves</b>	3
<b>IV. Detectability</b>	5
<b>V. Conclusions</b>	7
<b>Acknowledgments</b>	8
<b>References</b>	8

## I. INTRODUCTION

The era of gravitational wave astronomy has begun with the spectacular detection of gravitational waves from event GW150914 [1]. This detection not only established that advanced interferometers can indeed detect the tiny effect of gravitational waves reaching the detectors, but it also demonstrated that data analysis using numerical relativity can extract physical parameters of the underlying engine. Assuredly the various efforts on the experimental hardware, data analysis, and source modeling are now being pursued with even more ardor.

Although a black hole binary produced the first direct detection of gravitational waves, the merger of two neutron stars had long been a primary target for Advanced LIGO (aLIGO), and indeed a detection of a binary neutron star system is eagerly anticipated. One reason for this excitement is that neutron stars represent

a very extreme state of matter not accessible in the laboratory, and gravitational waves may reveal the equation of state (EoS) of matter at such extreme densities.

To understand what these gravitational waves tell us about the equation of state requires modeling the merger of these neutron stars, and such an effort spans a few techniques. A Post-Newtonian expansion of the two body problem is appropriate for the early orbiting stage of the merger while numerical relativity is needed for the near-merger, merger and post-merger phases [2]. Near coalescence (prior to the merger), numerical relativity is being used to enhance perturbative approaches (e.g. the effective one-body approach) in order to account for tidal effects—that depend on the EoS—in a concise and analytic manner [3].

The effects of the EoS become most significant as the stars approach each other and tidal forces grow. However, this regime is characterized by frequencies higher than those of the inspiral, and current detectors lose sensitivity for these increasing frequencies. Therefore, the extraction of the EoS from gravitational waves alone can be a subtle and difficult enterprise (e.g. [4, 5]).

Consequently, exploring the various pathways to extract physical information during the coalescence and post-merger stages is critical. These pathways include the search for gravitational wave features highly sensitive to the EoS. In addition, combining the complementary information provided by possible electromagnetic counterparts [6–8] may greatly increase the information we can extract from the gravitational wave signal alone.

One example of a gravitational wave feature that may lead to better understanding of the EoS concerns the frequency spectrum of the post-merger  $l = 2, m = 2$  mode. Several studies have found that this post-merger signal is characterized by a peak frequency that is related to the

underlying EoS [6, 9–11].

Beyond this dominant mode, recent work has also shown that a weaker but longer lived mode, the  $l = 2, m = 1$  mode, develops in the post-merger epoch of binary neutron star mergers. This possibility was first described in Refs. [12, 13] using Newtonian gravity, and more recently the growth of this mode has been found within full, general relativity simulations [14–17].

Although initially weaker than the  $l = 2, m = 2$ , the  $l = 2, m = 1$  has a couple compensating effects working for it. First, the  $m = 1$  mode occurs at roughly half the frequency of the dominant mode, and at this lower frequency the noise level is reduced with respect to that at higher frequencies[49]. Second, because the  $m = 1$  mode is less radiative and because it has hydrodynamic and magnetic instabilities helping support it, the mode is generally less damped than the  $m = 2$  mode, and its longer life yields more signal to detect. Furthermore, both these characteristic  $m = 1$  and  $m = 2$  modes are amenable to searches *triggered* by the strong inspiral detection. Moreover, the 2:1 frequency ratio of these two modes allows for an analysis of the correlation between the frequencies that may improve detectability.

In this note, we go extend the studies provided in [15, 17] on the development and detectability prospects of the  $m = 1$  mode. In particular we illustrate the behavior of this mode in the mergers of both equal and unequal mass binaries with different realistic, microphysical equations of state. We examine the effects of neutrino cooling and changes to the EoS, and find that even when accounting for the cooling due to neutrinos –which take away significant from the resulting object– the  $m = 1$  mode develops and grows to relevant strengths to impact the characteristics of the gravitational waves emitted by the system. By varying the mass ratio, we estimate the strength of this  $m = 1$  signal, and conclude that, as one would expect, the  $m = 1$  is much stronger for the unequal mass cases in the early stages after-merger. We also estimate the expected SNR and discuss detectability prospects. In particular we argue that such mode can be targeted following a triggered-search strategy. We summarize details of our implementation in section II, present results in section III, and conclude in section IV.

## II. NUMERICAL IMPLEMENTATION

The evolution equations for the spacetime and the fluid are described in our previous paper [9], while full details of our implementation are described in Ref. [18]. Unless otherwise specified, we adopt geometrized units where  $G = c = M_\odot = 1$ , except for some particular results which are reported more naturally in physical cgs units.

Einstein equations in the presence of both matter and radiation are,

$$G_{ab} = 8\pi(T_{ab} + \mathcal{R}_{ab}), \quad (1)$$

where  $T_{ab}$  is the stress energy tensor of a perfect fluid and

$\mathcal{R}_{ab}$  is the contribution from the radiation field. Our stars consist of a fluid described by the stress energy tensor

$$T_{ab} = hu_a u_b + Pg_{ab}, \quad (2)$$

where  $h$  is the fluid’s *total* enthalpy  $h \equiv \rho(1 + \epsilon) + P$ , and  $\{\rho, \epsilon, Y_e, u^a, P\}$  are the rest mass energy density, specific internal energy, electron fraction (describing the relative abundance of electrons compared to the total number of baryons), four-velocity, and pressure of the fluid, respectively.

To track the composition of the fluid and the emission of neutrinos we employ a leakage scheme. In particular, the equations of motion consist of the following conservation laws

$$\nabla_a T_b^a = \mathcal{G}_b, \quad (3)$$

$$\nabla^a (T_{ab} n^b) = 0, \quad (4)$$

$$\nabla_a (Y_e \rho u^a) = \rho R_Y, \quad (5)$$

where  $n^a$  is a timelike vector orthonormal to constant time surfaces employed to express Einstein equations as an initial value problem (e.g. [19]). The sources  $\mathcal{G}_a$  ( $\equiv -\nabla_c \mathcal{R}_a^c$ ) and  $R_Y$  correspond to the radiation four-force density and lepton source, respectively, and these quantities are computed within the leakage scheme. These equations are conservation laws for the stress-energy tensor, matter, and lepton number, respectively. Notice that, in the absence of lepton source terms ( $R_Y = 0$ ), Eq. (5) provides a conservation law for leptons and is similar to the familiar baryon conservation law, i.e.,  $Y_e$  is a mass scalar.

As mentioned, full details of our implementation can be found in Ref. [18], but a summary of our numerical techniques is included for completeness. We employ finite difference techniques on a regular, Cartesian grid to discretize the system. The geometric fields are discretized with a fourth order accurate scheme that satisfies summation by parts [20, 21], while a High-Resolution Shock-Capturing method based on the HLLE flux formulae with PPM reconstruction is used to discretize the hydrodynamical variables. The fluid equations are discretized with finite differences (rather than finite volume) as prescribed for the third-order ENO method [22, 23]. This simplifies coupling the fluid equations to the Einstein equations. The time evolution of the resulting equations adopts a third order accurate Runge-Kutta scheme [23, 24]. To provide sufficient resolution efficiently, we employ adaptive mesh refinement (AMR) via the HAD computational infrastructure. This infrastructure provides distributed, Berger-Oliger style AMR [25, 26] with full sub-cycling in time, as well as an improved treatment of artificial boundaries [27].

Importantly, we study these systems in 3D without imposing any symmetry condition that might suppress certain dynamics. For example, enforcing reflection symmetry in the equal mass, non-spinning case would necessarily exclude any odd  $m$  mode.

### III. RESULTS: DENSITY BEHAVIOR & GRAVITATIONAL WAVES

This note studies the post-merger stage of binary neutron star systems that have been the focus of our recent work [6, 9]. We extend these studies with the goal of examining more closely the development of an  $m = 1$  mode as a result of the merger of both equal and unequal mass cases.

The systems we study are consistent with current astrophysical observations (see e.g. Ref. [28]). Here, we consider binaries with the same total gravitational mass  $M = 2.70M_{\odot}$  but with different mass ratios,  $q \equiv M_1/M_2$ , ranging from  $q = 1$  (the equal mass case) to  $q = 0.76$ .

We concentrate on the three realistic EoS previously considered [50] in Refs. [6, 9]. These three EoS span a range of stiffnesses, from the softest (smallest neutron stars) SFHo [29], to the intermediate DD2 [30], and finally to the stiffest NL3 [30].

The physical parameters of the binaries and of our grid setup are summarized in Table I. Notice that for the total mass considered here, the hypermassive neutron star (HMNS) resulting from the SFHo merger collapses to a black hole roughly  $\approx 8$  ms after merger. Thus the associated SNR for the gravitational waves emitted after merger for this case will likely be lower than the other cases.

As discussed elsewhere (see e.g. Ref. [32] and references cited therein), the merger of neutron stars involves a violent collision in which the individual stars move at a large fraction of the speed of light ( $v \approx 0.3c$ ). The newly formed massive neutron star rotates differentially with a primarily quadrupolar structure that produces gravitational waves in the  $l = 2, m = 2$  mode. However, the one-armed spiral instability can develop so that the gravitational radiation includes an  $l = 2, m = 1$  component. The development of this mode is apparent in Fig. 1 which displays the strength of the two  $l = 2$  modes (as measured by the Newman-Penrose radiative scalar  $\Psi_4$ ) with the DD2 EoS for the three mass ratios considered here.

The one-armed instability leads to the rapid rise of the  $m = 1$  mode on a short time scale:  $\lesssim 1.5$  ms for the unequal mass cases and  $\lesssim 3$  ms for the equal mass case. The equal mass case demonstrates a longer timescale as a result of the intrinsic symmetry of non-spinning, zero-eccentricity, equal mass mergers. Indeed, for the instability to occur in the equal mass case, a mechanism is required to break the symmetry to allow for odd modes. Such a mechanism is naturally provided by the Kelvin-Helmholtz instability that arises in the contact region and in the associated turbulence [17, 33]; as well a type of magnetic (Tayler) instability can induce an  $m = 1$  perturbation [33, 34].

Naturally, as the mass ratio departs from equality the  $m = 1$  mode becomes stronger and saturates earlier. This qualitative behavior generally holds among all three EoS, as is apparent in Fig. 2 that presents both the  $m = 2$  and

$m = 1$  modes for  $q = 0.85$  for the three different EoS. In all three cases, the  $m = 1$  reaches its saturation value roughly  $\approx 1.5$  ms after the stars come into contact.

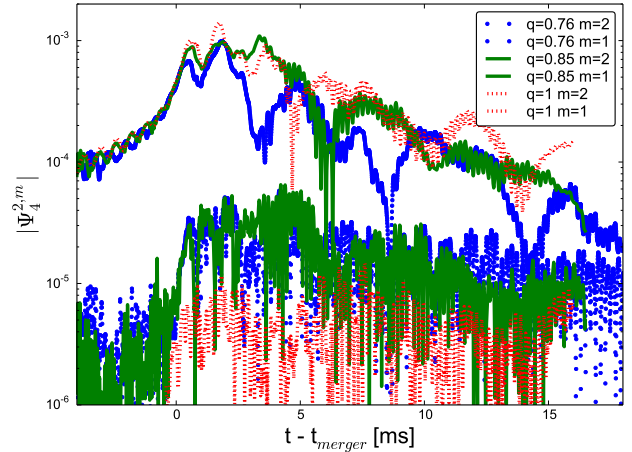


FIG. 1: The norm of a given mode ( $l = 2, m$ ) of the gravitational radiation described by  $\Psi_4^0$  as a function of time for different mass ratios with the DD2 EoS. Overall, the ( $l = 2, m = 1$ ) mode achieves saturation earlier for unequal mass than equal mass binaries. Notice that the  $m = 1$  modes decay more slowly with time than the corresponding ( $l = 2, m = 2$ ) modes. Here, the merger time is chosen when the stars first come into contact.

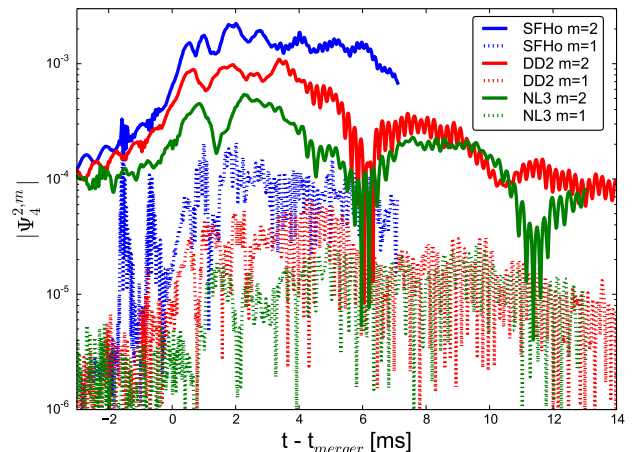


FIG. 2: Same as Fig. 1 for  $q=0.85$  with three different EoS (SFHo, DD2, NL3). Although the qualitative behavior is similar for all the cases, the strength of the signal is stronger for the softest EoS. Additionally, the decay rate of the  $m = 1$  mode has a mild dependence on the EoS though this observation might be affected by other physics effects—such as the Tayler instability. Notice that the remnant with the SFHo EoS collapses to a black hole roughly 8ms after merger.

This observed behavior is driven by the dynamics of the newly formed massive neutron star. Its fate will depend on the detailed structure of the object and, for ex-

EoS	$q$	$\nu$	$m_b^{(1)}, m_g^{(1)}$ [ $M_\odot$ ]	$m_b^{(2)}, m_g^{(2)}$ [ $M_\odot$ ]	$R^{(1)}$ [km]	$R^{(2)}$ [km]	$C^{(1)}$	$C^{(2)}$	$\Omega_0$ [rad/s]
NL3	0.85	0.248	1.34, 1.25	1.60, 1.47	14.75	14.8	0.125	0.147	1777
DD2	1.0	0.250	1.49, 1.36	1.49, 1.36	13.22	13.22	0.152	0.152	1776
DD2	0.85	0.248	1.36, 1.29	1.62, 1.47	13.20	13.25	0.144	0.164	1775
DD2	0.76	0.245	1.27, 1.18	1.71, 1.54	13.16	13.25	0.132	0.172	1775
SFHo	0.85	0.248	1.37, 1.25	1.63, 1.47	11.95	11.85	0.154	0.183	1773

TABLE I: Summary of the binary neutron star systems considered in this work. The initial data were computed using the BIN STAR solver from the LORENE package [31], with the assumption that the stars have an initial constant temperature of  $T = 0.02$  MeV and are in beta-equilibrium. All the binaries have a total mass  $M_0^{\text{ADM}} = 2.7M_\odot$  and start from an initial separation of 45 km. The outer boundary is located at 750 km and the highest resolution covering both stars is  $\Delta x_{\min} = 230m$ . The table displays the mass ratio of the binary  $q \equiv M_1/M_2$  and  $\nu = M_1 M_2 / M^2 = q/(q+1)^2$ , the baryon (gravitational) mass of each star  $m_b^{(i)}$  ( $m_g^{(i)}$ ), its circumferential radius  $R^{(i)}$  and its compactness  $C^{(i)}$  (i.e., when the stars are at infinite separation), the initial orbital angular frequency  $\Omega_0$ .

ample, its degree of differential rotation and continued susceptibility to instabilities. One useful avenue to begin the analysis of the global structure of the resulting hypermassive star is to construct cylindrical profiles of the star and decompose these profiles into Fourier amplitudes as was computed in Ref. [12], for example.

As an illustration of the density behavior and its qualitative change through time, Fig. 3 shows three such profiles extracted from the binary neutron star evolution with  $q = 0.85$  using the DD2 EoS. These profiles are extracted in three annuli in the equatorial plane, each with a width of 290 m and centered on radial distances of: 4.4 km (red curve), 7.4 km (black curve), and 10.3 km (blue curve) at times of 2.0 and 16.2 ms after merger in this system. The profiles use annuli that are evenly spaced in radius and use 32 evenly spaced azimuthal zones. A nearest cell algorithm is used to construct the average mass density profile. At the later point in the simulation, the remnant's structure is clearly dominated by a  $m = 1$  mode as the density profiles are well-matched by a single sine wave, though there is also power at higher  $m$  values as well, particularly at larger radii. One can also note that the maximum value in the profile shifts to slightly smaller azimuthal angle at increasing radius—indicative of the trailing, one armed spiral wave of a  $m = 1$  mode.

To help quantify this impression we perform a Fourier decomposition across the equatorial density distribution. We extract average density profiles in 10 evenly spaced annuli ranging in distance from 0.8 km to 4.8 km from the instantaneous center of mass with a width of 370 m across 32 evenly spaced azimuthal zones. These profiles are then transformed to extract complex amplitudes,  $C_m$ . The time evolution of these Fourier coefficients shows similar behavior across the 10 annuli and, for simplicity, we plot only the coefficients for one annulus in the middle of the set at a radius of 3.3 km in Fig. 4. The coefficients are normalized by the maximum value of the DC ( $m = 0$ ) coefficient in the annulus over the course of the simulation.

The middle panel of Fig. 4 shows Fourier coefficients

for the simulation with  $q = 0.85$  initially. After merger, the  $m = 1$  begins to dominate, as already indicated in the plot of the density profiles in Fig. 3. The  $m = 2$  mode decays indicating that the hypermassive star does not form a bar (again, confirming the profiles in Fig. 3) while both the  $m = 3$  and the eventually numerically dominated  $m = 4$  mode show similar decaying behavior (at a slightly higher rate than the  $m = 2$  mode). The bottom panel shows the analysis for the  $q = 0.76$  case, which are similar to that for the  $q = 0.85$  case. For the symmetric binary, shown in the top plot of Fig. 4, the  $m = 2$  bar mode dominates the post-merger evolution for  $\approx 15\text{ms}$ , though an  $m = 1$  has comparable power at the end of the simulation. This behavior is expected because it takes time for the turbulence to break the symmetry allowing the  $m = 1$  to develop. Hence, at first contact, the  $m = 1$  is essentially zero. In contrast, an  $m = 1$  component is already present at first contact due to the asymmetry of the unequal mass case. Nevertheless, as mentioned, after about a few ( $\approx 5$ ) rotation periods of the merged object the mode has saturated, and it overtakes the  $m = 2$  mode in roughly 20 rotation periods.

Interestingly, the frequency of the  $m = 1$  gravitational wave mode appears insensitive to the mass ratio,  $q$ , but is dependent on the EoS. We obtain the  $m = 1$  frequencies from Fourier decompositions  $\Psi_4$  (as shown in Fig. 5 for the DD2 case), and obtain  $f_{m1} \approx 1.0, 1.25, 1.7\text{kHz}$  for NL3, DD2, and SFHo, respectively. Importantly these frequencies are half that of the dominant  $m = 2$  mode for the same EoS ( $f_{\text{peak}} \approx 2, 2.5, 3.3\text{kHz}$ ) and therefore fall in a higher sensitivity band, albeit with (initially) a lower strain. Furthermore, the measured values for  $f_{m1}$  agree with the rotational frequencies of the remnant densities.

Before examining the detectability, we comment on the decay rates of the  $m = 1$  mode. In particular, while initially stronger than the  $m = 1$  mode, the  $m = 2$  decays at a faster rate. We estimate the decay rate to be  $\approx t^{-4\pm0.5}$  for the  $m = 2$  mode of  $|\Psi_4|$  while for the  $m = 1$  mode  $\approx t^{-1.5\pm1}$ . These exponents depend mildly on the mass ratio  $q$ , as apparent in Fig. 2. A precise estimate of the rates is beyond the scope of this note be-

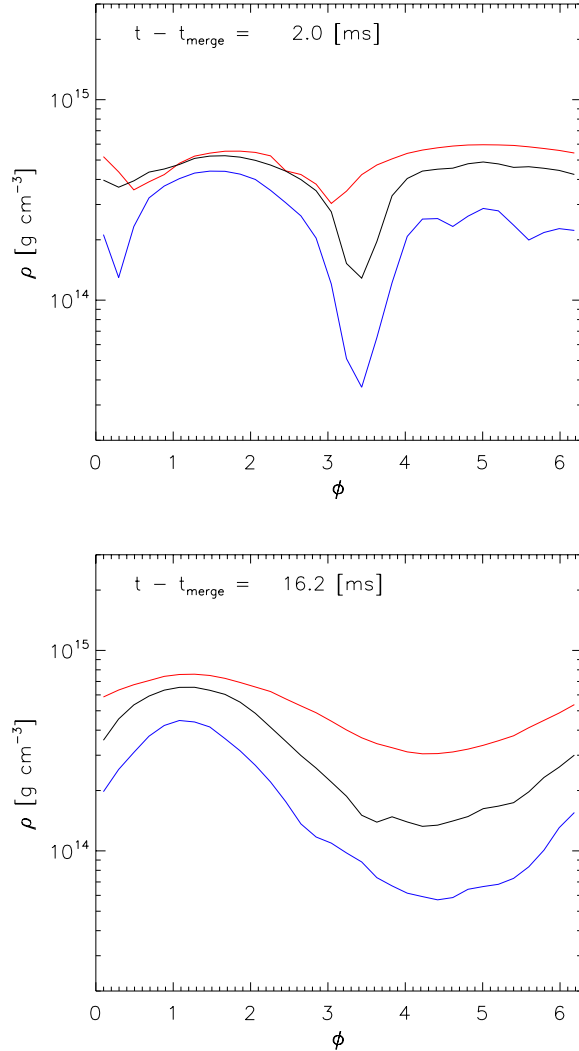


FIG. 3: The panels show three profiles of the average mass density in the equatorial plane, extracted from annuli of width 290m centered on the origin at radii of 4.4km (red curve), 7.4km (black curve), and 10.3km (blue curve) from the  $q = 0.85$  simulation with DD2 EoS. The density profiles  $\approx 2$ ms after merger (**top panel**) indicate a strong,  $m = 2$  bar mode modulation; at  $\approx 16$ ms (**bottom panel**) on the other hand, the density variations are dominated by a single  $m = 1$  mode. The eigenmode can be seen to have a trailing spiral character as the peak in the profile shifts to slightly smaller azimuth as the radius increases.

cause of their dependence on a variety of physical effects such as EoS, magnetohydrodynamics (requiring very high numerical resolution), and, depending on the lifetime of the remnant, transport effects that might become significant. Nevertheless, the  $m = 1$  mode is clearly more weakly damped than the  $m = 2$ , indicating the latter will overtake it (see also the discussion in [15, 17]).

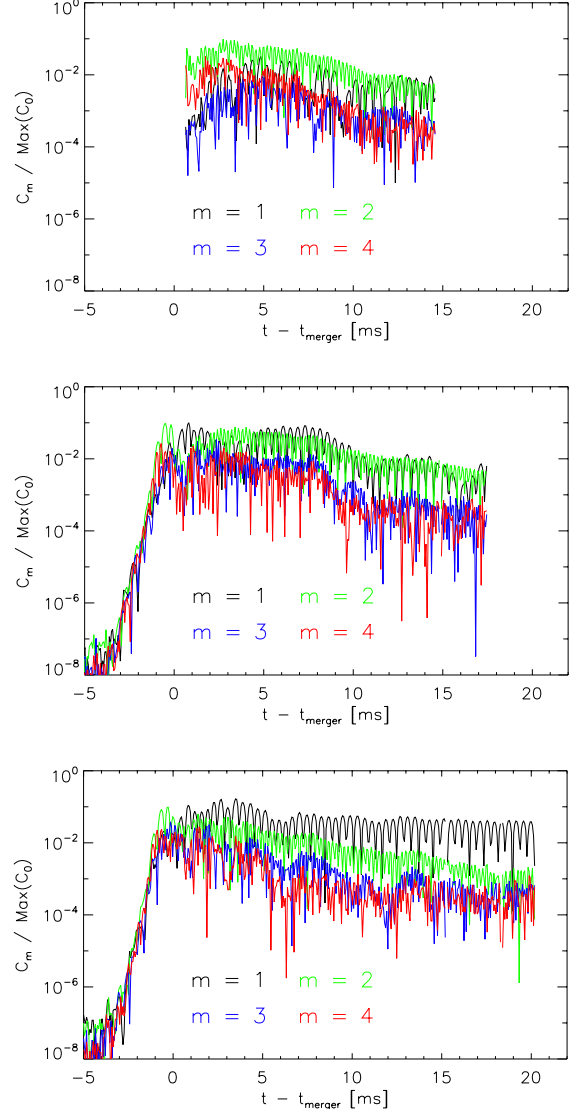


FIG. 4: Fourier decomposition of rest mass density extracted from an annulus at 3.3 km and 370 m wide about the instantaneous center of mass from simulations of a symmetric binary (**top panel**), a binary with mass ratio of  $q = 0.85$  (**middle panel**) and  $q = 0.76$  (**bottom panel**). These three simulations were evolved with the DD2 EoS. The amplitude of modes with  $m$  from 1 to 4 are shown normalized by the largest value of the 0th component of the Fourier decomposition in the annulus.

#### IV. DETECTABILITY

As described above, the  $m = 1$  mode grows rapidly and saturates with a mostly constant frequency and with an amplitude that decays slowly. For sufficiently massive systems, this mode ends when a black hole forms. For cases that do not promptly collapse, the lifetime can easily be  $T \gtrsim 20$ ms. A precise value for  $T$  depends on the details of the system such as the total mass and the

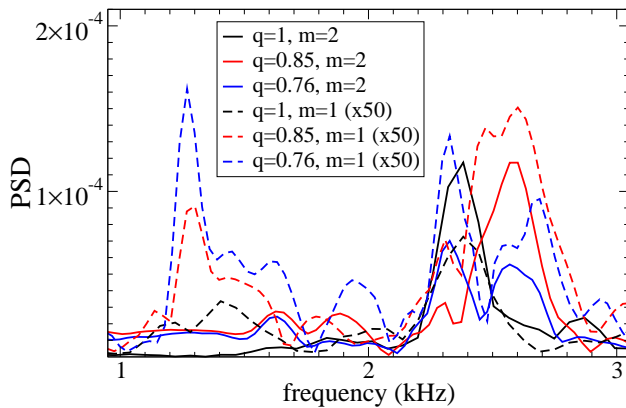


FIG. 5: Fourier transform of the  $\Psi_4^0$ -modes ( $l = 2, m$ ) shown in Fig. 1 for the DD2 EoS. For this EoS, the dominant radiative mode after merger is the ( $l = 2, m = 2$ ) mode, peaking at a frequency  $f_{\text{peak}} = 2.3\text{--}2.6$  kHz. Notice that, in contrast, the ( $l = 2, m = 1$ ) mode peaks around  $f_{m1} \approx f_{\text{peak}}/2 \approx 1.3$  kHz. This peak becomes more prominent for small mass ratios.

particular EoS. Also important are the dynamics of the remnant that could transport angular momentum outward and reduce thermal pressure support via cooling. Although an estimate of the neutrino cooling is considered in these simulations with a leakage scheme, we are not accounting for magnetic and radiation transport effects, which could potentially affect the  $m = 1$  mode over timescales of order  $\approx 100$  ms. Thus, in the following we adopt a conservative baseline lifetime of  $T = 10$  ms.

To estimate the SNR that such a mode would produce, we make use of the analysis described in Ref. [35]. The SNR  $\rho$  of a monochromatic gravitational wave with strain  $h = |\Psi_4^0|/(LM_\odot\omega^2)$  [recall, asymptotically  $\Psi_4 = \Psi_4^0/r + \mathcal{O}(r^{-2})$ ], at a fixed gravitational wave frequency  $f = \omega/(2\pi)$  (from a source at a distance  $L$ ) in a time window  $[T_i, T_f]$ , can be estimated by

$$\rho^2 \simeq \frac{2}{S_n(f)} \int_{T_i}^{T_f} h^2 dt. \quad (6)$$

The noise strain of the detector is denoted by  $\sqrt{S_n(f)}$  and given in units of  $\sqrt{\text{Hz}^{-1}}$ .

In all our examined cases corresponding to the DD2 EoS, the frequencies  $f_{m1}$  of  $m = 1$  modes agree with those measured from the orbital rotation rates. Additionally, we will assume a typical value  $|\Psi_{4_{m=1}}^0| \approx 5 \times 10^{-5}$  as observed in our simulations. With the exception of the SFHo case which collapses to a black hole roughly 8 ms after merger, the other cases result in a long-lived remnant that we have evolved for at least 15 ms post-merger (Ref. [36] has followed the equal-mass DD2 case for  $\approx 30$  ms after merger).

Using Eq. 6 and *assuming a constant strain*, we arrive at an estimate of the SNR for the  $m = 1$  mode for a

source at a horizon distance  $L$  as,

$$\rho_{m=1} \approx 11 \times \left[ \frac{6 \times 10^{-24} \text{Hz}^{-1/2}}{\sqrt{S_n(f_{m1})}} \right] \left[ \frac{|\Psi_{4_{m=1}}^0|}{5 \times 10^{-5}} \right] \left[ \frac{1.3 \text{kHz}}{f_{m1}} \right]^2 \left[ \frac{T}{10 \text{ms}} \right]^{1/2} \left[ \frac{10 \text{Mpc}}{L} \right] \quad (7)$$

where we have used for aLIGO  $\sqrt{S_n(f = 1.3 \text{kHz})} \approx 6 \times 10^{-24} \text{Hz}^{-1/2}$  (as per the zero-detuned, high laser power (no signal-recycling mirror) noise curve estimated in [37]).

Longer times will increase the SNR, and for scenarios with constant strain, the SNR would increase as  $\sqrt{T/10 \text{ms}}$ . The evolutions of Ref. [17] suggested that the strain can indeed be fairly constant for resolutions equal or better than  $\Delta x \approx 222$  m (while they see decay for  $\Delta x = 295$  m). Our resolution,  $\Delta x = 230$  m, is comparable though it could be possible that the rates of decay measured would decrease further with higher resolution. We caution however that for long-time scales other physics will come into play—for example cooling and angular momentum transfer—thus at this point it is difficult to draw firm conclusions on timescales longer than  $\approx 20$  ms. At a conservative level, however, we can employ the decay rate we observe here for the  $m = 1$  mode,  $\propto t^{-1.5}$ , and estimate the SNR for  $t \in [3, 20]$  ms as

$$\rho_{m=1} \approx 2 \times \left[ \frac{6 \times 10^{-24} \text{Hz}^{-1/2}}{\sqrt{S_n(f_{m1})}} \right] \left[ \frac{|\Psi_{4_{m=1}}^0(3 \text{ms})|}{5 \times 10^{-5}} \right] \left[ \frac{1.3 \text{kHz}}{f_{m1}} \right]^2 \left[ \frac{10 \text{Mpc}}{L} \right]. \quad (8)$$

This value is certainly lower (at a given distance) than that assuming a constant magnitude in Eq. (7) but is nevertheless significant.

As a figure of merit, we can compare the SNR of the  $m = 1$  mode to the  $m = 2$  mode using the same assumptions. In particular, assuming the  $m = 1$  and  $m = 2$  modes emit at a constant frequency and with decay rates given by  $\propto \{t^{-1.5}, t^{-4}\}$  respectively, and also making use of the fact that the noise curve of aLIGO grows approximately linearly with increasing frequency. The ratio of the corresponding SNRs in a time window  $[T_i, T_f]$ , results in

$$\begin{aligned} \frac{\rho_{m=1}}{\rho_{m=2}} &= \frac{\sqrt{S_n(2f_0)}}{\sqrt{S_n(f_0)}} \frac{|h_{m=1}(T_i)|}{|h_{m=2}(T_i)|} \sqrt{\frac{14}{4}} \sqrt{\frac{(1 - (T_i/T_f)^2)}{(1 - (T_i/T_f)^7)}} \\ &\approx 13 \frac{|\Psi_{4_{m=1}}^0(T_i)|}{|\Psi_{4_{m=2}}^0(T_i)|}. \end{aligned} \quad (9)$$

Therefore, if at  $t = T_i$ , the  $m = 1$  mode strength of  $\Psi_4^0$  is at least a thirteenth of the strength of the  $m = 2$  mode, it will become more relevant than the  $m = 2$  as a contributor to the post-merger gravitational wave signal (a condition that would be even less strict if the  $m = 1$  mode decays at a slower rate).

The estimate obtained in Eq. 7 is not, at first sight, encouraging for possible detection in a single event. However, close binaries with a very long lived  $m = 1$  mode would be the most promising for this task, and of course future detectors and upgrades of current detectors will naturally improve prospects for detecting this post-merger signal. However, we argue here that approaching the detection of the  $m = 1$  mode using *triggered search strategies* significantly enhances the prospects. The detection of the inspiral signal from a distant neutron star binary would provide timing estimates and physical parameters. In particular knowledge of the total mass, in turn, will inform whether a long lived remnant is probable. This information would allow for the same sort of aggressive data analysis and reduced detection thresholds as occur in follow-ups of electromagnetic triggers [38–40]. The inspiral would serve as the trigger for both the post-merger  $m = 1$  and  $m = 2$  analysis, which can be correlated, and this trigger would allow for a decreased threshold in SNR for detection. In particular assuming a detection threshold in SNR of  $\approx 1$ , then Eq. 7 yields a horizon distance as high as  $100 \text{ Mpc} [\sqrt{T/10\text{ms}}]$  (again, assuming that the mode maintains a constant strain for that time period).

The detection of both modes will provide information about the EoS. The observation that the  $m = 1$  mode frequency is half that of the  $m = 2$  mode means that the peak frequencies of both modes encode information about the EoS as has been demonstrated for the  $m = 2$  modes in recent work [6, 41, 42]. For instance, Ref. [6] finds a fit for this peak frequency

$$f_{\text{peak}}[\text{kHz}] = -1.61 + 2.96 f_c \left[ \frac{2.7M_\odot}{M} \right] [\text{kHz}] \quad (10)$$

in terms of the “contact” frequency  $f_c$ . This frequency is strongly dependent on the EoS and is defined in terms of the gravitational masses involved,  $m_g^{(1)}$  ( $M_g = m_g^{(1)} + m_g^{(2)}$ ) and their compaction ratio  $C_i$

$$f_c = \frac{1}{\pi M_g} \left( \frac{m_g^{(1)}}{M_g C_1} + \frac{m_g^{(2)}}{M_g C_2} \right)^{-3/2}. \quad (11)$$

Data analysis can be directed to look for a correlated signal in these two modes that may improve the extraction of the encoded EoS information.

## V. CONCLUSIONS

The evolutions presented here, as well as those in Refs. [15, 17], indicate that the one-armed spiral instability develops generically in the merger of binary neutron stars (that do not promptly collapse to a black hole). Our analysis includes both (non spinning) equal and unequal mass binaries described by realistic equations of state. We find that this instability develops for a broad range

of EoS ranging from soft to stiff, though its strength is weaker for stiff EoS than for soft ones. For the equal mass cases, the instability is seeded by turbulence while in the unequal mass cases the  $m = 1$  mode is seeded strongly from the onset because of the inherent asymmetry of the system. In agreement with Refs. [15, 17] we find that the mode grows quickly and saturates in just a few rotational periods of the newly formed object. For unequal mass mergers within  $\lesssim 14 \text{ Mpc} [\sqrt{T/10\text{ms}}]$ , the strength of the mode is sufficient for a *direct detection* (i.e. with  $\text{SNR} \geq 8$ ) by aLIGO with planned sensitivities (in particular with the so-called “zero-detuned, high laser power (no signal-recycling mirror)” configuration) provided the mode stays roughly constant in strength. If this mode decays as estimated in this work  $\propto t^{-1.5}$ , the horizon distance for detection is reduced to  $\simeq 3 \text{ Mpc}$  though this decay could be reduced in higher resolution studies (see [17]).

The time for the  $m = 1$  mode to reach saturation naturally depends on the asymmetry of the merger which, for non-spinning binary neutron stars, is determined by the mass ratio of the binary. Even in equal mass, symmetric encounters this time is observed to be at most 4 ms. Although the strain of the  $m = 1$  mode in all cases roughly 4 ms after merger is weaker than the dominant,  $m = 2$  mode, its strain can be as large as  $\approx 50\%$  of the main  $l = 2, m = 2$  mode. Furthermore the ratio of strain in the  $m = 1$  to  $m = 2$  modes grows with time and becomes larger than unity after  $\approx 20 - 30$  ms (for systems that do not collapse to a black hole within this timeframe). The  $m = 1$  mode also benefits from having a frequency half that of the  $m = 2$  mode where aLIGO has less noise (the noise curve grows roughly quadratically in frequency in this region frequency region). Because of the slower decay time and smaller frequency, the SNRs of both modes become roughly comparable and that of the  $m = 1$  should dominate at late enough times.

We have also presented a more hopeful prospect for detection than in Ref. [17]. Because gravitational waves from the inspiral of a binary neutron star system would be detectable by aLIGO/VIRGO at distances of a few 100s of megaparsecs, the search for the post-merger  $m = 1, 2$  modes would proceed as in a triggered-search. In particular, because we have a good estimate both of the mode frequencies and of their timescales, such an analysis would be quite well targeted. A Bayesian analysis may be able to extract characteristic features from the post-merger signal as long as differences of  $\mathcal{O}(1)$  arise from the assumption of various priors motivated by the dynamics discussed here. Thus a targeted analysis may significantly extend the reach of the modest distance assumed in Eq. 7. Finally, the 2:1 connection of the peak frequencies of these two modes with the EoS could enable stacking different signals and enhance the possibility of extracting these modes.

The detection of these modes would complement a detection of the pre-merger inspiral, providing more information about the EoS. As recent work has shown, the

post-merger remnant demonstrates a characteristic frequency peak that is intimately related to the underlying EoS [6, 41–45].

We have studied the  $m = 1$  spiral arm instability that, along with the  $m = 2$  mode, encodes important information about the post-merger remnant and its EoS. The dynamics of the  $m = 1$  mode are important for its ultimate detection by both current and future detectors, and it is therefore important to better understand the impact of various effects including cooling, transport of angular momentum, and magnetic instabilities. Further work on these fronts is ongoing [46].

Vasileos Paschalidis, and Frans Pretorius for interesting discussions as well as our collaborators Eric Hirschmann, David Neilsen, and Marcelo Ponce. This work was supported by NSF grant PHY-1308621 (LIU), NASA’s ATP program through grant NNX13AH01G, NSERC through a Discovery Grant (to LL) and CIFAR (to LL). CP acknowledges support from the Spanish Ministry of Education and Science through a Ramon y Cajal grant and from the Spanish Ministry of Economy and Competitiveness grant FPA2013-41042-P. Research at Perimeter Institute is supported through Industry Canada and by the Province of Ontario through the Ministry of Research & Innovation. Computations were performed at XSEDE and Scinet.

### Acknowledgments

It is a pleasure to thank William East, Gabriela Gonzalez, Chad Hanna, Sascha Husa, Francisco Jimenez,

- 
- [1] **Virgo, LIGO Scientific** Collaboration, B. . Abbott *et al.*, “Observation of Gravitational Waves from a Binary Black Hole Merger,” *Phys. Rev. Lett.* **116** no. 6, (2016) 061102, [arXiv:1602.03837 \[gr-qc\]](#).
  - [2] J. A. Faber and F. A. Rasio, “Binary Neutron Star Mergers,” *Living Rev. Rel.* **15** (2012) 8, [arXiv:1204.3858 \[gr-qc\]](#).
  - [3] T. Hinderer *et al.*, “Effects of neutron-star dynamic tides on gravitational waveforms within the effective-one-body approach,” [arXiv:1602.00599 \[gr-qc\]](#).
  - [4] B. D. Lackey and L. Wade, “Reconstructing the neutron-star equation of state with gravitational-wave detectors from a realistic population of inspiralling binary neutron stars,” *Phys. Rev.* **D91** no. 4, (2015) 043002, [arXiv:1410.8866 \[gr-qc\]](#).
  - [5] M. Agathos, J. Meidam, W. Del Pozzo, T. G. F. Li, M. Tompitak, J. Veitch, S. Vitale, and C. V. D. Broeck, “Constraining the neutron star equation of state with gravitational wave signals from coalescing binary neutron stars,” *Phys. Rev.* **D92** no. 2, (2015) 023012, [arXiv:1503.05405 \[gr-qc\]](#).
  - [6] L. Lehner, S. L. Liebling, C. Palenzuela, O. L. Caballero, E. O’Connor, M. Anderson, and D. Neilsen, “Unequal mass binary neutron star mergers and multimessenger signals,” [arXiv:1603.00501 \[gr-qc\]](#).
  - [7] Y. Sekiguchi, K. Kiuchi, K. Kyutoku, and M. Shibata, “Dynamical mass ejection from binary neutron star mergers: Radiation-hydrodynamics study in general relativity,” *Phys. Rev.* **D91** no. 6, (2015) 064059, [arXiv:1502.06660 \[astro-ph.HE\]](#).
  - [8] S. Rosswog, “The multi-messenger picture of compact binary mergers,” *Int. J. Mod. Phys.* **D24** no. 05, (2015) 1530012, [arXiv:1501.02081 \[astro-ph.HE\]](#).
  - [9] C. Palenzuela, S. L. Liebling, D. Neilsen, L. Lehner, O. L. Caballero, E. O’Connor, and M. Anderson, “Effects of the microphysical equation of state in the mergers of magnetized neutron stars with neutrino cooling,” *Phys. Rev. D* **92** no. 4, (Aug., 2015) 044045, [arXiv:1505.01607 \[gr-qc\]](#).
  - [10] W. Kastaun and F. Galeazzi, “Properties of hypermassive neutron stars formed in mergers of spinning binaries,” *Phys. Rev. D* **91** no. 6, (Mar., 2015) 064027, [arXiv:1411.7975 \[gr-qc\]](#).
  - [11] F. Foucart, R. Haas, M. D. Duez, E. O’Connor, C. D. Ott, L. Roberts, L. E. Kidder, J. Lippuner, H. P. Pfeiffer, and M. A. Scheel, “Low mass binary neutron star mergers : gravitational waves and neutrino emission,” [arXiv:1510.06398 \[astro-ph.HE\]](#).
  - [12] S. Ou and J. Tohline, “Unexpected dynamical instabilities in differentially rotating neutron stars,” *Astrophys. J.* **651** (2006) 1068–1078, [arXiv:astro-ph/0604099 \[astro-ph\]](#).
  - [13] G. Corvino, L. Rezzolla, S. Bernuzzi, R. De Pietri, and B. Giacomazzo, “On the Shear Instability in Relativistic Neutron Stars,” *Class. Quant. Grav.* **27** no. 11, (2010) 114104, [arXiv:1001.5281 \[gr-qc\]](#).
  - [14] M. Anderson, E. W. Hirschmann, L. Lehner, S. L. Liebling, P. M. Motl, D. Neilsen, C. Palenzuela, and J. E. Tohline, “Magnetized Neutron-Star Mergers and Gravitational-Wave Signals,” *Physical Review Letters* **100** no. 19, (May, 2008) 191101, [arXiv:0801.4387 \[gr-qc\]](#).
  - [15] W. E. East, V. Paschalidis, F. Pretorius, and S. L. Shapiro, “Relativistic Simulations of Eccentric Binary Neutron Star Mergers: One-arm Spiral Instability and Effects of Neutron Star Spin,” *Phys. Rev.* **D93** no. 2, (2016) 024011, [arXiv:1511.01093 \[astro-ph.HE\]](#).
  - [16] T. Dietrich, N. Moldenhauer, N. K. Johnson-McDaniel, S. Bernuzzi, C. M. Markakis, B. Brgmann, and

- W. Tichy, “Binary Neutron Stars with Generic Spin, Eccentricity, Mass ratio, and Compactness - Quasi-equilibrium Sequences and First Evolutions,” *Phys. Rev.* **D92** no. 12, (2015) 124007, [arXiv:1507.07100 \[gr-qc\]](https://arxiv.org/abs/1507.07100).
- [17] D. Radice, S. Bernuzzi, and C. D. Ott, “The One-Armed Spiral Instability in Neutron Star Mergers and its Detectability in Gravitational Waves,” [arXiv:1603.05726 \[gr-qc\]](https://arxiv.org/abs/1603.05726).
- [18] D. Neilsen, S. L. Liebling, M. Anderson, L. Lehner, E. OConnor, *et al.*, “Magnetized Neutron Stars With Realistic Equations of State and Neutrino Cooling,” *Phys. Rev.* **D89** no. 10, (2014) 104029, [arXiv:1403.3680 \[gr-qc\]](https://arxiv.org/abs/1403.3680).
- [19] L. Lehner, “Numerical relativity: A Review,” *Class. Quant. Grav.* **18** (2001) R25–R86, [arXiv:gr-qc/0106072 \[gr-qc\]](https://arxiv.org/abs/gr-qc/0106072).
- [20] G. Calabrese *et al.*, “Novel finite-differencing techniques for numerical relativity: Application to black hole excision,” *Class. Quant. Grav.* **20** (2003) L245–L252, [gr-qc/0302072](https://arxiv.org/abs/gr-qc/0302072).
- [21] G. Calabrese, L. Lehner, O. Reula, O. Sarbach, and M. Tiglio, “Summation by parts and dissipation for domains with excised regions,” *Class. Quant. Grav.* **21** (2004) 5735–5758, [gr-qc/0308007](https://arxiv.org/abs/gr-qc/0308007).
- [22] C.-W. Shu and S. Osher, “Efficient implementation of essentially non-oscillatory shock-capturing schemes,” *J. Comput. Phys.* **77** no. 2, (1988) 439–471.
- [23] M. Anderson, E. Hirschmann, S. L. Liebling, and D. Neilsen, “Relativistic MHD with adaptive mesh refinement,” *Class. Quant. Grav.* **23** (2006) 6503–6524, [gr-qc/0605102](https://arxiv.org/abs/gr-qc/0605102).
- [24] M. Anderson *et al.*, “Simulating binary neutron stars: dynamics and gravitational waves,” *Phys. Rev.* **D77** (2008) 024006, [arXiv:0708.2720 \[gr-qc\]](https://arxiv.org/abs/0708.2720).
- [25] HAD home page <http://had.liu.edu>, 2010.
- [26] S. L. Liebling, “The singularity threshold of the nonlinear sigma model using 3d adaptive mesh refinement,” *Phys. Rev. D* **66** (2002) 041703.
- [27] L. Lehner, S. L. Liebling, and O. Reula, “AMR, stability and higher accuracy,” *Class. Quant. Grav.* **23** (2006) S421–S446, [arXiv:gr-qc/0510111](https://arxiv.org/abs/gr-qc/0510111).
- [28] J. M. Lattimer, “The nuclear equation of state and neutron star masses,” *Annual Review of Nuclear and Particle Science* **62** no. 1, (2012) 485–515, <http://dx.doi.org/10.1146/annurev-nucl-102711-095018>.
- [29] A. W. Steiner, M. Hempel, and T. Fischer, “Core-collapse Supernova Equations of State Based on Neutron Star Observations,” *ApJ* **774** (Sept., 2013) 17, [arXiv:1207.2184 \[astro-ph.SR\]](https://arxiv.org/abs/1207.2184).
- [30] M. Hempel, T. Fischer, J. Schaffner-Bielich, and M. Liebendörfer, “New Equations of State in Simulations of Core-collapse Supernovae,” *ApJ* **748** (Mar., 2012) 70, [arXiv:1108.0848 \[astro-ph.HE\]](https://arxiv.org/abs/1108.0848).
- [31] LORENE. home page <http://www.lorene.obspm.fr/>, 2010.
- [32] L. Lehner and F. Pretorius, “Numerical Relativity and Astrophysics,” *Ann.Rev.Astron.Astrophys.* **52** (2014) 661–694, [arXiv:1405.4840 \[astro-ph.HE\]](https://arxiv.org/abs/1405.4840).
- [33] M. Anderson *et al.*, “Magnetized Neutron Star Mergers and Gravitational Wave Signals,” *Phys. Rev. Lett.* **100** (2008) 191101, [arXiv:0801.4387 \[gr-qc\]](https://arxiv.org/abs/0801.4387).
- [34] H. C. Spruit, “Differential rotation and magnetic fields in stellar interiors,” *A&A* **349** (Sept., 1999) 189–202, [astro-ph/9907138](https://arxiv.org/abs/astro-ph/9907138).
- [35] P. Jaranowski, A. Krolak, and B. F. Schutz, “Data analysis of gravitational - wave signals from spinning neutron stars. 1. The Signal and its detection,” *Phys. Rev.* **D58** (1998) 063001, [arXiv:gr-qc/9804014 \[gr-qc\]](https://arxiv.org/abs/gr-qc/9804014).
- [36] Y. Sekiguchi, K. Kiuchi, K. Kyutoku, M. Shibata, and K. Taniguchi, “Dynamical mass ejection from the merger of asymmetric binary neutron stars: Radiation-hydrodynamics study in general relativity,” [arXiv:1603.01918 \[astro-ph.HE\]](https://arxiv.org/abs/1603.01918).
- [37] “Ligo document t0900288-v3.” <https://dcc.ligo.org/cgi-bin/DocDB/ShowDocument?docid=2974>.
- [38] **VIRGO, LIGO Scientific** Collaboration, B. Abbott *et al.*, “Astrophysically Triggered Searches for Gravitational Waves: Status and Prospects,” *Class. Quant. Grav.* **25** (2008) 114051, [arXiv:0802.4320 \[gr-qc\]](https://arxiv.org/abs/0802.4320).
- [39] A. Dietz, N. Fotopoulos, L. Singer, and C. Cutler, “Outlook for detection of GW inspirals by GRB-triggered searches in the advanced detector era,” *Phys. Rev.* **D87** no. 6, (2013) 064033, [arXiv:1210.3095 \[gr-qc\]](https://arxiv.org/abs/1210.3095).
- [40] **VIRGO, LIGO Scientific** Collaboration, J. Aasi *et al.*, “Search for long-lived gravitational-wave transients coincident with long gamma-ray bursts,” *Phys. Rev.* **D88** no. 12, (2013) 122004, [arXiv:1309.6160 \[astro-ph.HE\]](https://arxiv.org/abs/1309.6160).
- [41] A. Bauswein and N. Stergioulas, “A unified picture of the post-merger dynamics and gravitational wave emission in neutron-star mergers,” *ArXiv e-prints* (Feb., 2015) , [arXiv:1502.03176 \[astro-ph.SR\]](https://arxiv.org/abs/1502.03176).
- [42] S. Bernuzzi, T. Dietrich, and A. Nagar, “Modeling the Complete Gravitational Wave Spectrum of Neutron Star Mergers,” *Physical Review Letters* **115** no. 9, (Aug., 2015) 091101, [arXiv:1504.01764 \[gr-qc\]](https://arxiv.org/abs/1504.01764).
- [43] T. Dietrich, S. Bernuzzi, M. Ujevic, and B. Brgmann, “Numerical relativity simulations of neutron star merger remnants using conservative mesh refinement,” *Phys. Rev.* **D91** no. 12, (2015) 124041, [arXiv:1504.01266 \[gr-qc\]](https://arxiv.org/abs/1504.01266).
- [44] A. Bauswein, N. Stergioulas, and H.-T. Janka, “Exploring properties of high-density matter through remnants of neutron-star mergers,” *Eur. Phys. J.* **A52** no. 3, (2016) 56, [arXiv:1508.05493 \[astro-ph.HE\]](https://arxiv.org/abs/1508.05493).
- [45] L. Rezzolla and K. Takami, “Gravitational-wave signal from binary neutron stars: a systematic analysis of the spectral properties,” [arXiv:1604.00246 \[gr-qc\]](https://arxiv.org/abs/1604.00246).
- [46] E. W. Hirschmann, P. Motl, and et.al., “ $m = 1$  instabilities in binary neutron star mergers.”
- [47] P. Demorest, T. Pennucci, S. Ransom, M. Roberts, and J. Hessels, “Shapiro Delay Measurement of A Two Solar Mass Neutron Star,” *Nature* **467** (2010) 1081–1083, [arXiv:1010.5788 \[astro-ph.HE\]](https://arxiv.org/abs/1010.5788).
- [48] J. Antoniadis, P. C. Freire, N. Wex, T. M. Tauris, R. S. Lynch, *et al.*, “A Massive Pulsar in a Compact Relativistic Binary,” *Science* **340** (2013) 6131, [arXiv:1304.6875 \[astro-ph.HE\]](https://arxiv.org/abs/1304.6875).
- [49] At frequencies beyond  $\approx$ kHz the detector noise increases quadratically with frequency.
- [50] These three EoS are capable of producing neutron stars with masses of at least  $2 M_{\odot}$ , and they are thus

consistent with current observations of NS masses [47, 48].